ELSEVIER

Journal of Fluids and Structures 25 (2009) 506–518

JOURNAL OF FLUIDS AND STRUCTURES

www.elsevier.com/locate/jfs

Experimental investigation of flow through a bank of cylinders of varying geometry

S. Gilchrist*, S. Green

Department of Mechanical Engineering, The University of British Columbia, Vancouver, Canada V6T 1Z4

Received 10 October 2006; accepted 11 October 2008
Available online 6 March 2009

Abstract

An experimental investigation of a model forming fabric was conducted. The forming fabric was simplified and represented by a bank of two rows of cylinders. Particle image velocimetry (PIV), pressure drop, and hydrogen bubble visualization were used to evaluate the upstream and gross flow patterns for various diameter ratios and cylinder spacings at a Reynolds number of 65. It was found that for a row separation of 0.75 times the upstream cylinder diameter, the upstream flow matched that for a single row of cylinders. Further, it was found that when the pressure drop through the bank of cylinders was equal to the sum of the individual rows' pressure drops, the upstream flow converged to that of a single row.

Keywords: Cylinder; Bank; Forming fabric; PIV

1. Introduction

Papermaking is a multistage, continuous process that contains three fundamental procedures carried out in succession: forming, pressing and drying. On the forming end of the paper machine a dilute suspension of pulp in water, generally about 0.7% pulp by mass, is drained through a forming fabric to create a pulp mat. This mat is then passed on to the press section where water is removed through direct pressure, and finally into the dryer section where the last of the water is removed through heat and convection. Fig. 1 shows a schematic of the forming section of a paper machine where the stock suspension is sprayed in a long, thin jet through the forming fabric before being passed to the press section.

In order to create a high quality, even density sheet of paper, the drainage of the water from the suspension must occur uniformly. For this reason, a significant amount of development has gone into forming fabrics that allow fast and even drainage, and have high fibre retention. This development was complicated by the need to have different characteristics on each side of the fabric. A fine structure is required on the papermaking surface (the "paper side", filaments ~0.15 mm diameter) to provide ample support for the pulp fibres, and a coarse structure (filaments ~0.3 mm diameter) is required on the surface in contact with the papermaking machine (the "machine side") to increase wear life and decrease running resistance. In fluid mechanics terminology, the machine side is the downstream side of the forming fabric. These characteristics can be seen in Fig. 2.

*Corresponding author.
E-mail address: seth@mech.ubc.ca (S. Gilchrist).

0889-9746/$ - see front matter © 2008 Elsevier Ltd. All rights reserved.
doi:10.1016/j.jfluidstructs.2008.10.001

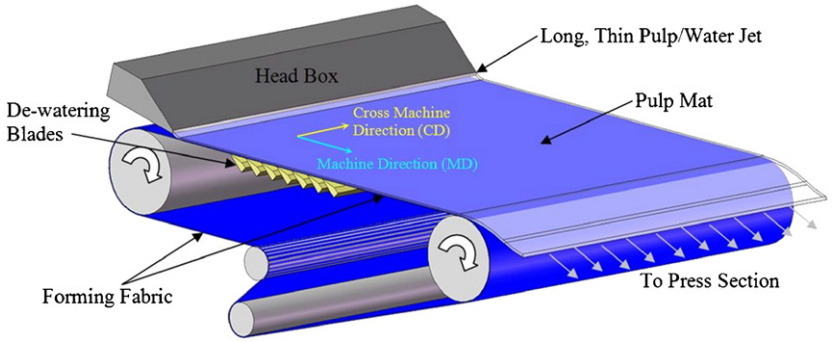

Fig. 1. The forming section of a paper machine.

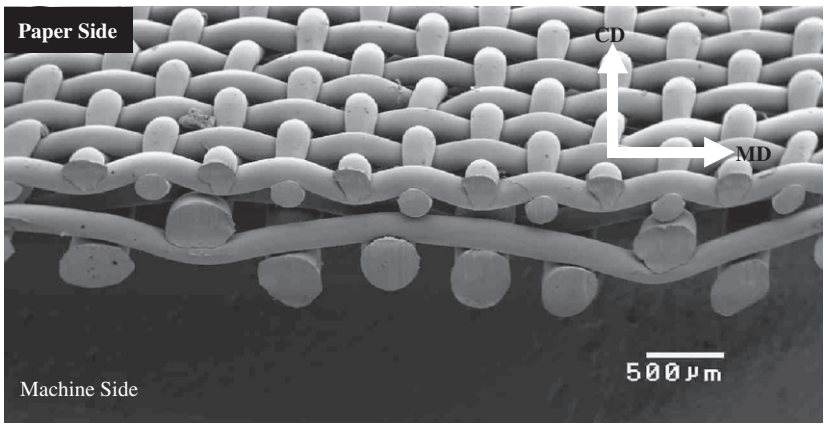

Fig. 2. A micrograph showing the two sides of a forming fabric. Photo courtesy of Asten Johnson.

The two-sidedness of forming fabrics makes it difficult to predict drainage rate and fibre retention. This difficulty has led to the use of engineering techniques and tools in forming fabric performance analysis. The current research is concerned with experimental examination of the flow field in the vicinity of the forming fabric paper-side surface with the goal of finding easily measurable characteristics, such as the pressure drop through the fabric, which may indicate non-uniformities in the flow field.

In order to experimentally investigate forming fabric flow structures, some simplifications were required to reduce the complexity of the problem. In reality, papermaking flows are multiphase and three-dimensional; however, a survey of the forming fabric literature allows for reasonable engineering simplifications to make the problem more manageable, yet still applicable.

Before beginning a discussion of the simplifications, a brief explanation will be made of common forming fabric terminology and how this equates to fluid mechanics terms. Forming fabrics are described by three unit vectors, oriented with the direction that the fabric is mounted on the paper machine. As shown in Fig. 1, the machine direction (MD) is oriented in the direction of fabric motion, along the paper machine axis. The second direction, the cross-machine direction (CD), is in the plane of the forming fabric, and is orthogonal to the MD. The third direction is the z-direction and is normal to the forming fabric surface, with z positive in the direction from the machine side to the paper side of the fabric.

There are many other terms to describe the characteristics of the weave and geometry of the fabric that have not been discussed here (such as shed, plane difference, open area, etc.), but the basic geometric terms presented above should allow the reader to understand the following simplifications.

(1) Due to the low concentration of pulp fibres, the interaction of the fibres with each other and with the bulk flow field can be neglected (Parker, 1972). This results in modelling the flow as pure water, reducing the complexity by removing the second phase.

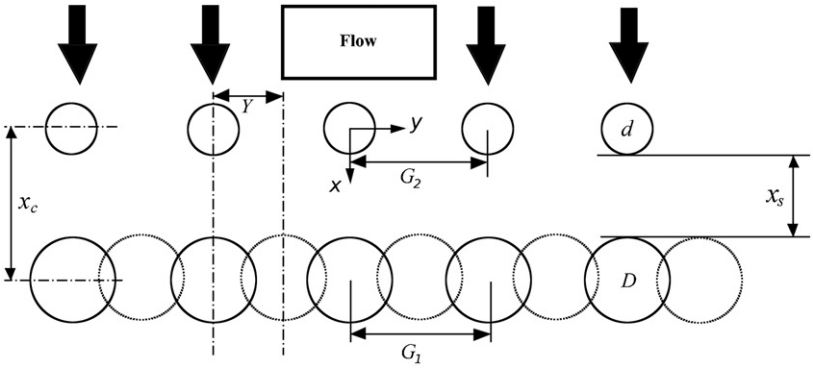

Fig. 3. Cylinder bank geometry and nomenclature, adapted from Huang (2003). Flow is in the x-direction.

(2) A number of researchers have investigated the influence of pulp fibre orientation and interaction with the forming fabric. The hydrodynamics of the headbox tend to orient the fibres in the streamwise (machine) direction (Olson, 2002). With the fibres oriented in the MD, the CD filaments (which are perpendicular to the fibre long axis) provide more support points than the filaments that are parallel to the fibre. As a result of this increased support, the CD filaments play a more critical role in the determination of the structure of the pulp mat than the MD filament geometry. This result has been confirmed by a number of other investigations, most notably by Johnson in 1986 and Adanur in 1994 (Beran, 1979; Johnson, 1986; Adanur, 1994; Helle, 1978). The current research therefore represents the complex three-dimensional geometry of real forming fabrics as a two-dimensional bank of dissimilar cylinders representing the CD papermaking fabric filaments.

The final flow parameter to be determined is the Reynolds number. Research conducted on flow velocities in the initial drainage region shows that the z-direction velocity varies from 0.05 to 0.50 m/s depending on impingement angle, position, and headbox jet velocity (Dalpke et al., 2004). This results in a Reynolds number between 6.5 and 65 based on the paper-side filament diameter, with the higher value occurring earlier in the deposition process, before the pulp mat retards the flow.

The above simplifications result in the flow investigated here: the two-dimensional flow of pure water through a bank of two parallel rows of cylinders oriented perpendicular to the free stream. These cylinders have differing sizes and spacings, and the Reynolds number of the flow based on upstream cylinder diameter is between 6.5 and 65 (Fig. 3).

In Fig. 3, the diameter of the upstream cylinders is designated d and is used as the cylinder bank's characteristic length for Reynolds number calculation and nondimensionalization. The diameter of the downstream row cylinders is designated D. The y-direction cylinder separation in the upstream row is designated G_1 with the nondimensional G_1/d being represented by g_1. In the downstream row G_2 represents the cylinder spacing with g_2 being the nondimensional form. The separation of the rows is designated X_S for surface separation and X_C for center separation. In the current research, X_S is more commonly used than X_C. The quantity Y represents the cylinder centre off-set between the upstream row and downstream rows. This is designated only for cases of $G_1 = G_2$ since when $G_1 \neq G_2$, Y is a function of the cylinders under inspection.

2. Literature review

Due to their relevance, flows through banks of cylinders have been well studied and are, for the most part, well understood. Flows that concern single cylinders and banks of similar cylinders at moderate Reynolds numbers have received the most attention due to their frequent occurrence in heat transfer and vibration analysis (Bearman and Wadcock, 1973; Williamson, 1985; Kim and Durbin, 1988; Polak and Weaver, 1995; Sumner et al., 1999, 2000; Ziada, 2000; Alam et al., 2003). There are also a number of studies that investigate similar geometries at higher Reynolds numbers (Braun, 1995; Roychowdhury et al., 2002; Iwaki et al., 2004; Gal et al., 1996). However, even with all the work that has been done, there are still aspects of flows through banks of cylinders that are not well understood. These include flows at low Reynolds number, flows through banks of cylinders of nonuniform sizing and spacing, and examination of the flow upstream of a bank of cylinders, all of which are of particular interest in forming fabric applications.

While the current literature is focused on the higher Reynolds number regime, examination of the literature allows for the postulation of expected flow structures and mechanisms. The flow through the bank of cylinders is complex. The proximity of the rows of cylinders creates flow fields with numerous interactions. Sumner et al. (2000) has identified a number of different cylinder interactions for pairs of staggered and tandem cylinders. The tandem cylinders were seen to interact in one of three ways, when they were close or in contact ($0 \leqslant X_S/d \leqslant 0.1$, given in terms of X_C in the reference) they acted as a single bluff body, as separation increased past $X_S/d = 0.1$ the cylinders were seen to interact through shear layer reattachment when the shear layer from the upstream cylinder would impinge upon, and reattach to the downstream cylinder. The resulting flow pattern is similar to the bluff body pattern with a single set of alternating Kármán vortices and a single Strouhal number. This flow pattern was maintained until $X_S/d = 3.0$ when the dominating pattern was vortex impingement, where the vortices generated by the upstream cylinder impinge directly on the downstream cylinder.

For the 45° staggered configurations ($Y/G_1 = 0.5$), the bluff body flow field was again seen when the cylinders were in close proximity but as X_S/d rose above 0.1 a flow pattern characterized by vortex pairing, splitting and subsequent enveloping was seen. Once the centre separation reached $X_S/d \geqslant 0.5$ the wakes did not interact, but the cylinders' vortex shedding was synchronised, indicating that the systems were still coupled.

The pressure drops of tandem cylinders in cross-flow were investigated by Alam et al. (2003). In his investigation, pressure measurements were made at different angles from the free stream and drag coefficients were calculated for various cylinder separations. Alam's drag results coincide well with Sumner's results with a step change in the drag coefficient occurring at $X_S/d = 3$, which is where Sumner identified a shift to vortex impingement.

Huang (2003) and Huang et al. (2006) have carried out a numerical investigation of two-dimensional flow through banks of similar and dissimilar cylinders at various separations and staggerings at low Reynolds numbers. Huang found that the second row of cylinders had little effect upstream of the bank of cylinders for a row surface separation of 0.7 times the upstream cylinder diameter or more ($X_S/d \geqslant 0.7$).

3. Experimental methods

The experiments were carried out in the University of British Columbia, Pulp and Paper Centre water/glycerine flow loop. The loop can provide velocities from 2 to 10 cm/s in the 30 cm × 30 cm test-section. Using a glycerol solution with a viscosity between 12 and 18 cP, and cylinder diameters such that end effects could be neglected (Gal et al., 1996), the test-section Reynolds number range was nominally 10–65.

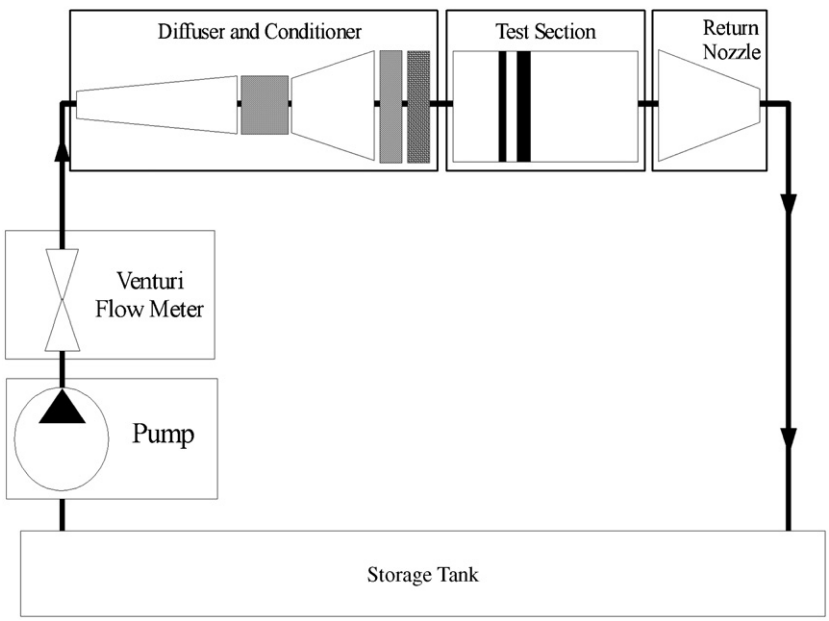

Fig. 4. UBC Pulp and Paper Centre glycerine/water flow loop.

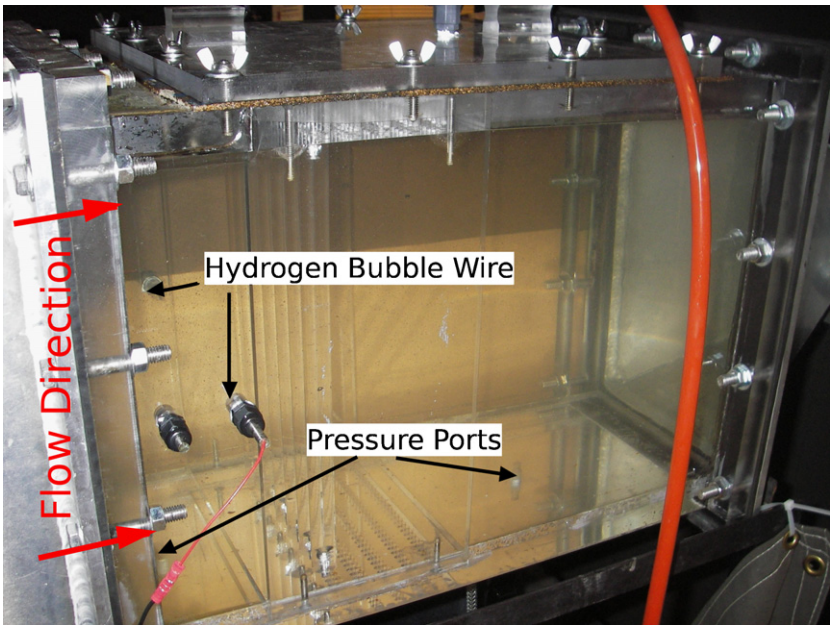

Fig. 5. The 30×30 cm test-section showing the location of the static pressure ports, hydrogen bubble generation wire and the cylinder bank frame.

The flow loop was a closed configuration. It was driven by a 20 hp electric pump with velocity measurement via a Venturi flow meter located downstream of the pump. The flow passed through a series of diffusers, conditioning screens and a honeycomb flow straightener before entering the test-section. It then returned to the storage tank via a large diameter return line. A schematic of the flow loop is shown in Fig. 4.

The test-section was constructed of acrylic to facilitate PIV observation. It had ports for static pressure data acquisition, and was fitted with a 0.002 in diameter platinum wire for hydrogen bubble generation. The bank of cylinders was supported by a configurable frame that could hold various arrangements and sizes of upstream and downstream cylinders. An image of the test-section is shown in Fig. 5.

There were three main methods of data collection: particle image velocimetry (PIV), static pressure drop, and hydrogen bubble visualization. The PIV was used to give near instantaneous flow field observations and was oriented such that the laser shadow was in the wake region of the cylinder bank. The pressure drop measurements were made using a low-differential pressure sensor calibrated for a range of 0–0.1 in of water (0–25 Pa) differential pressure. Measurements were taken between a location upstream of the cylinder bank and one downstream of the cylinder bank on the bottom of the test-section. The hydrogen bubble generation wire was located at the test-section mid-line just upstream of the cylinder bank.

Flow in the test-section was observed with the hydrogen bubble generation wire to be even to within 5% over 83% of the test-section, with boundary layers being a bit less than 2 cm thick (6.67% of test-section width) at the location of the cylinder bank. These observations were made using a high-definition video camera at multiple velocities.

4. PIV results and discussion

A number of configurations were evaluated using PIV. In order to keep the plots uncluttered only one uncertainty bar has been included on each plot. The bars represent the maximum uncertainty for 80% confidence. The plots were smoothed using a moving average and in some cases a polynomial fit with a 10% span.

The location of the PIV data is $d/4$ upstream of the bank of cylinders. To orient the reader, Fig. 6 shows a vector plot of the data for $D/d = 3$, $Y/G_1 = 0.5$, (staggered), $G_2/G_1 = 2$, $X_S/d = 0$, and $\mathrm{Re} = 65$.

Fig. 6 shows the optical distortion obtained in the shadow region behind the cylinder bank. Additionally, since the PIV laser is aimed at the mid-plane of the test-section, the ends of the cylinders closest to the camera are out of focus and out of alignment with the vector data. The corresponding line plot of this data is shown in Fig. 11. It is evident from

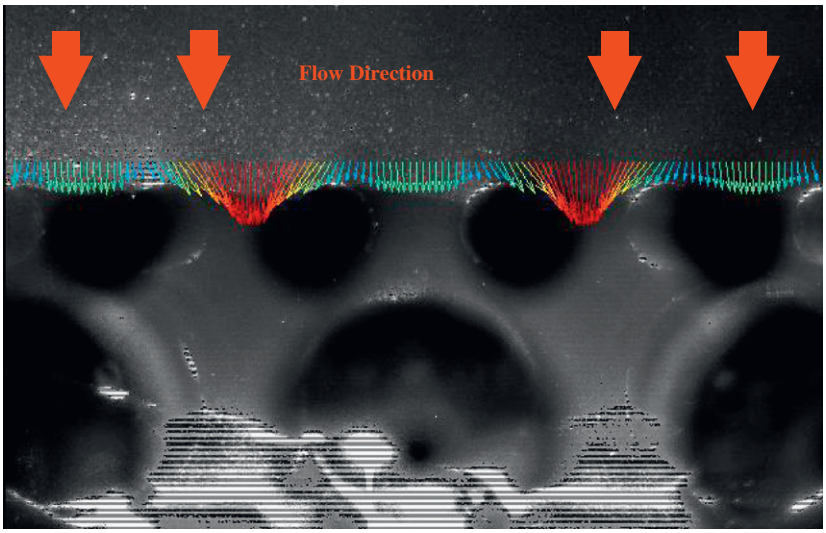

Fig. 6. A vector plot from the PIV system of the velocities $d/4$ upstream of the cylinder bank.

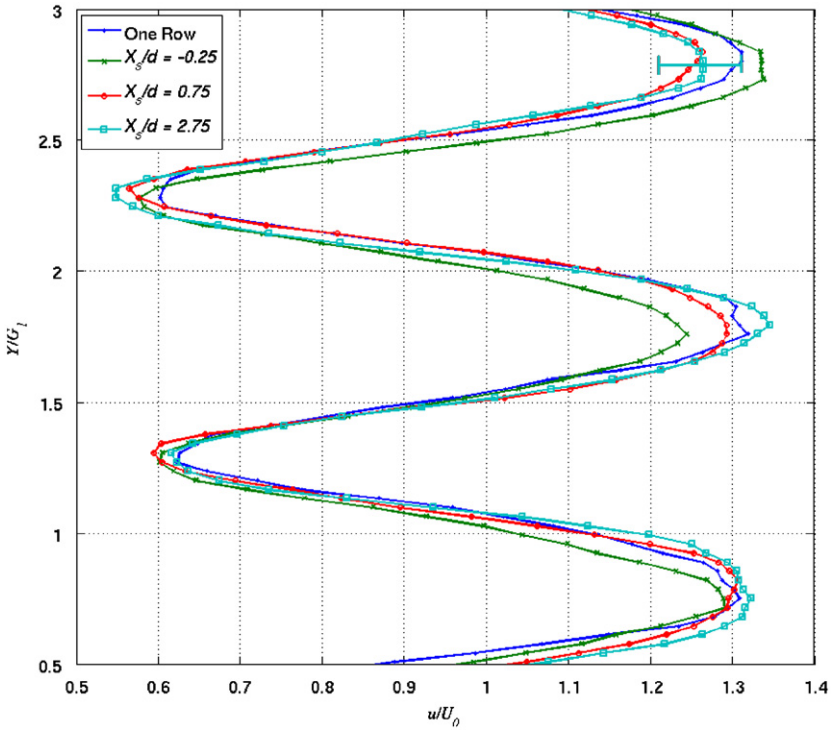

Fig. 7. Streamwise velocity for various X_S/d for $D/d = 1.5$, $G_2/G_1 = 1$, $Y/G_1 = 0.5$ at $\mathrm{Re} = 65$.

these figures that uncertainty and comparisons between configurations are more easily displayed on a line plot, and for these reasons the data will be shown in line plots.

Fig. 7 shows the effects on the streamwise component when changing the surface separation, X_S, for an arrangement of $D/d = 1.5$, $G_2/G_1 = 1$, and $Y/G_1 = 0.5$, at $\mathrm{Re} = 65$. The cross-stream component of the same arrangement is shown in Fig. 8. In both plots the velocities are statistically identical.

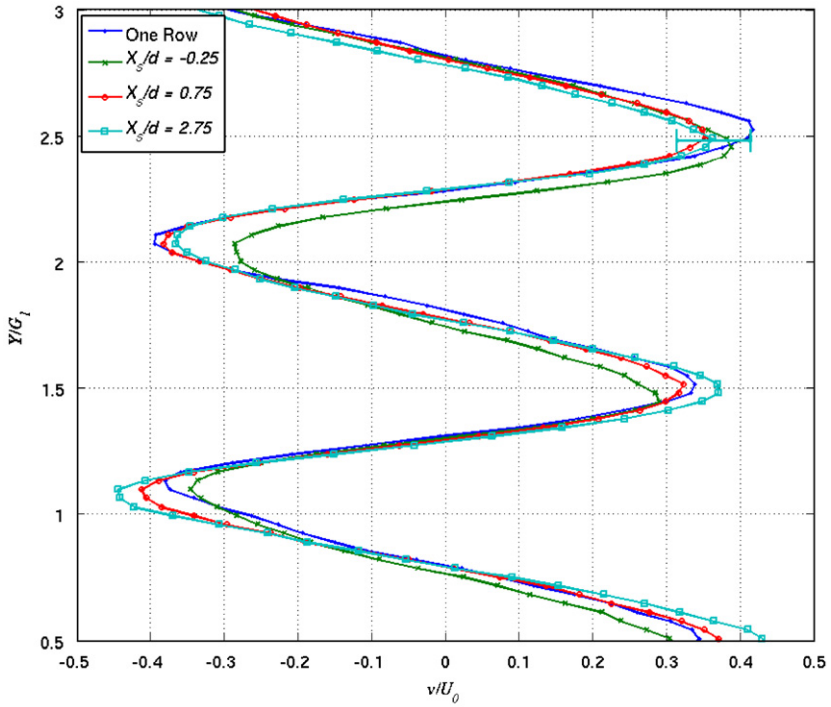

Fig. 8. Cross-stream velocity for various X_S/d for $D/d = 1.5$, $G_2/G_1 = 1$, $Y/G_1 = 0.5$ at $\mathrm{Re} = 65$.

Figs. 7 and 8 show that for $G_2/G_1 = 1$, changing X_S had little effect on the upstream flow pattern. Further, Figs. 9 and 10 show that for $G_2/G_1 = 1$ and $X_S/d = 0.75$, variations in Y/G_1 had negligible effect on the flow $d/4$ upstream of the rows of cylinders. This result agrees with Huang, who found that for $X_S/d = 0.7$ and $\mathrm{Re} = 65$ variations in staggering had no effect on the upstream flow field.

The results shown in Fig. 11 indicate that staggering had a much more significant influence than cylinder diameter ratio or relative row spacing when the two rows were in full contact. $D/d = 3$ was the largest diameter ratio tested and even when the two rows of cylinders were in full contact no change was observed in the upstream flow pattern until staggering was introduced.

5. ΔP results and discussion

Due to the complicated nature of PIV data collection and analysis, only extreme cases were evaluated. Pressure drop data were more straightforward to collect and analyze so all of the cases shown in the PIV results, as well as a number of additional, intermediate configurations were evaluated.

The pressure drop coefficient was calculated using

$$k = \frac{\Delta P}{\frac{1}{2}\rho U^2}. \tag{1}$$

The uncertainty bars shown in the k results were most significantly influenced by the measurement of velocity, which itself had an uncertainty of $\pm 3\%$. Since U^2 is in the denominator of Eq. (1), test-section velocity contributes disproportionately to the uncertainty of k.

Fig. 12 shows the pressure drop coefficient as a function of X_S/d for a configuration of $D/d = 1.5$, $G_2/G_1 = 1$, and $Y/G_1 = 0.5$ at $\mathrm{Re} = 65$. The negative value of X_S/d indicates that the leading edge of the downstream cylinder was upstream of the trailing edge of the upstream cylinder. This was only possible for staggered configurations. The pressure drop through the bank of cylinders for this configuration converged to the sum of the individual rows' pressure drops by $X_S/d = 0.75$. Fig. 13 shows the pressure drop coefficient through the same bank of cylinders as in Fig. 12, but with

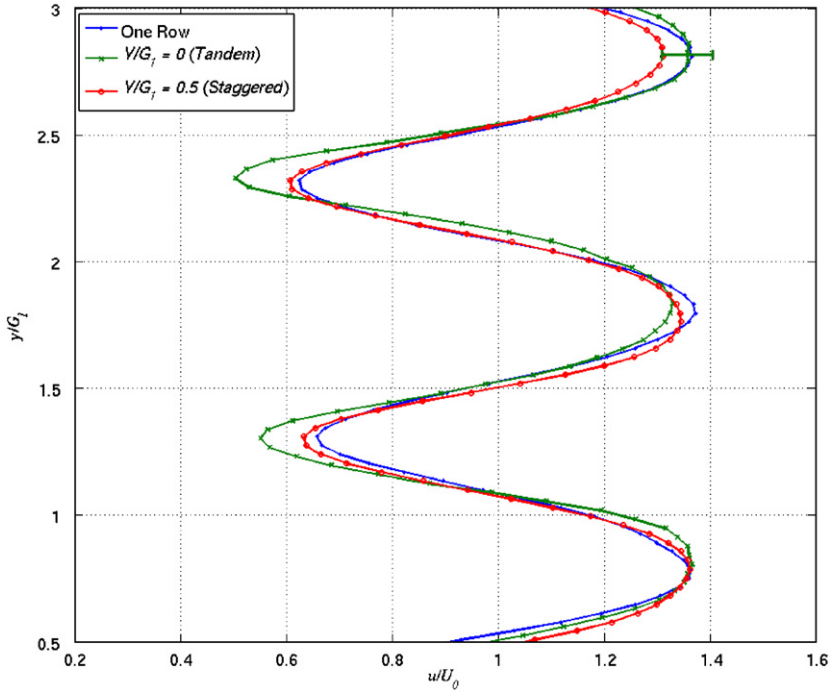

Fig. 9. Streamwise velocities for changing Y/G_1 and $D/d = 1.5$, $G_2/G_1 = 1$, $X_S/d = 0.75$ at $\mathrm{Re} = 65$.

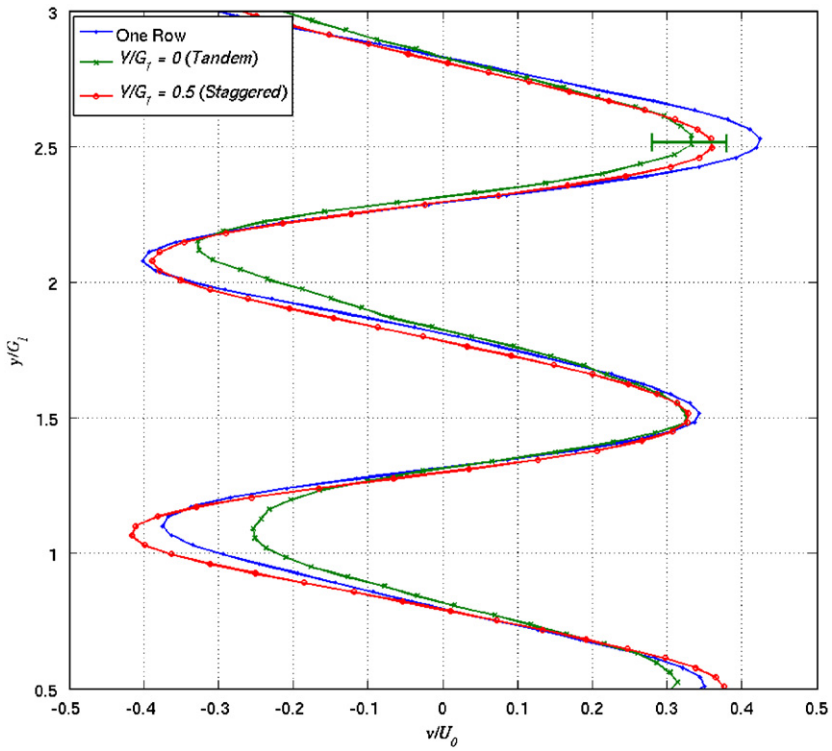

Fig. 10. Cross-stream velocities for changing Y/G_1 and $D/d = 1.5$, $G_2/G_1 = 1$, $X_S/d = 0.75$ at $\mathrm{Re} = 65$.

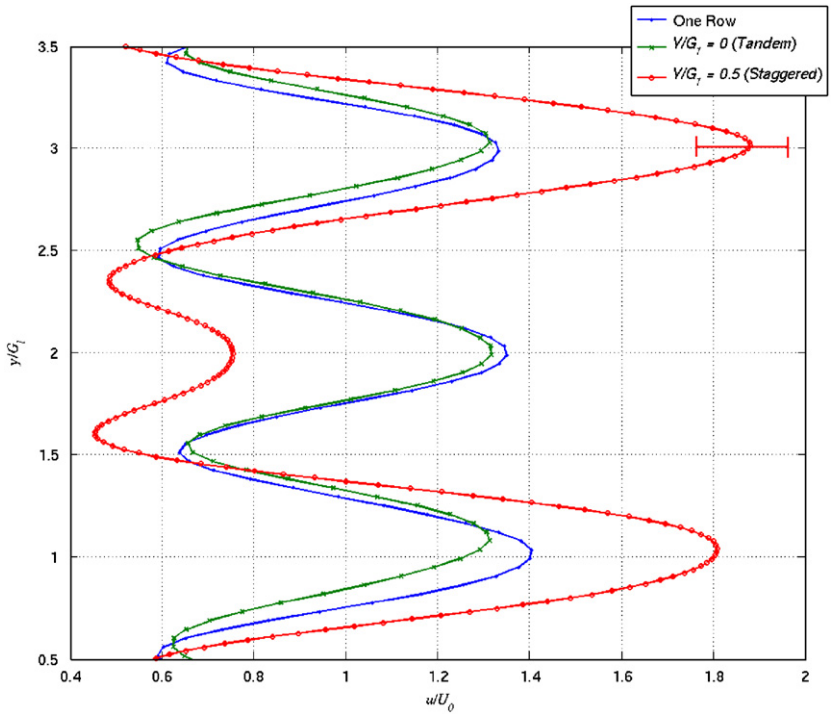

Fig. 11. Streamwise velocity component for variations in staggering with $D/d = 3$, $G_2/G_1 = 2$, $X_s/d = 0$ at $\mathrm{Re} = 65$.

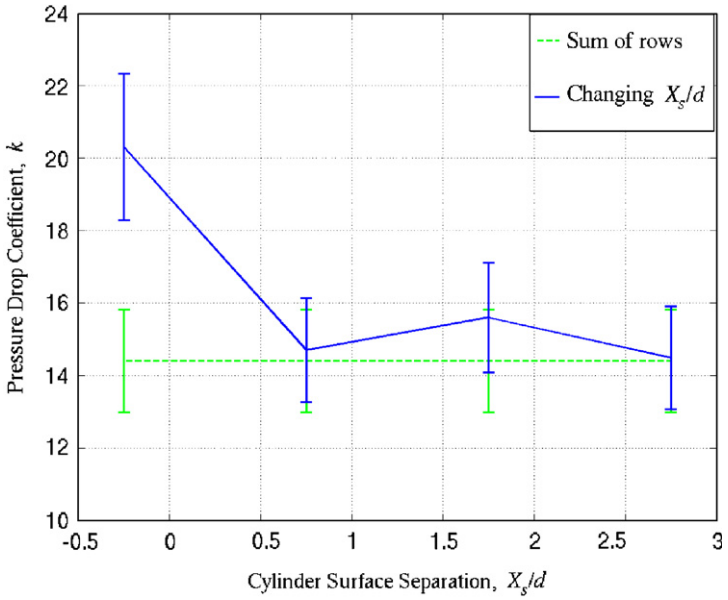

Fig. 12. Pressure drop as a function of row separation for $D/d = 1.5$, $G_2/G_1 = 1$, $Y/G_1 = 0.5$ and $\mathrm{Re} = 65$.

$Y/G_1 = 0$. Here too, the pressure drop is independent of the row separation for $X_S/d \geqslant 0.75$; for $X_S/d \geqslant 0.75$ the flow through each row of cylinders was essentially independent.

Fig. 14 shows the pressure drop as a function of staggering for $D/d = 1.5$, $G_2/G_1 = 1$, and $X_S/d = 0.75$ at $\mathrm{Re} = 65$. The pressure drop coefficient was independent of the row staggering. When this data is considered in conjunction with the PIV data shown in Figs. 9 and 10 it is seen that the upstream flow fields were also independent of staggering.

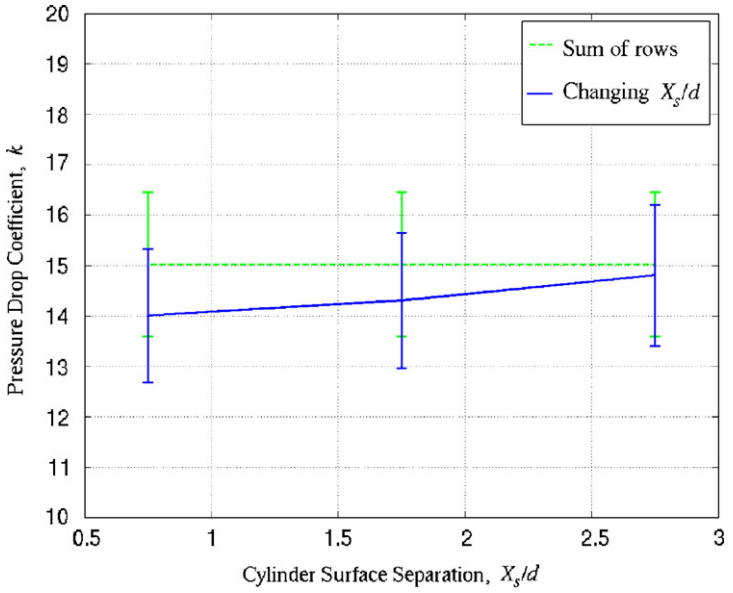

Fig. 13. Pressure drop as a function of row separation for $D/d = 1.5$, $G2/G1 = 1$, $Y/G_1 = 0$ and $\mathrm{Re} = 65$.

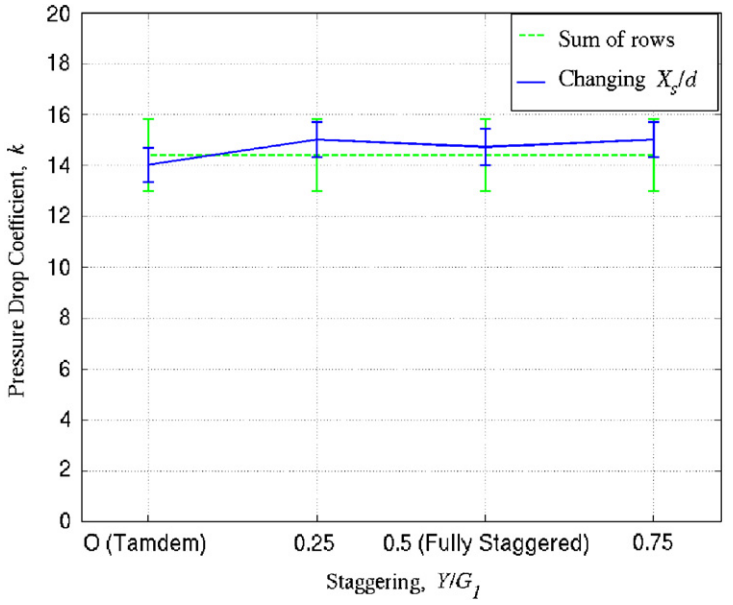

Fig. 14. Pressure drop as a function of staggering for $D/d = 1.5$, $G_2/G_1 = 1$, $X_S/d = 0.75$ at $\mathrm{Re} = 65$.

Fig. 15 shows the pressure drop coefficient as a function of X_S/d with $G_1 \neq G_2$. Even with unequal row spacing the pressure drop coefficient converged to the sum of the rows' pressure drops for $X_S/d \geqslant 0.75$.

The pressure drop coefficient as a function of Reynolds number for staggered and tandem configurations is plotted in Fig. 16. k decreases monotonically with Re, as one would expect at these low Reynolds numbers. Additionally, the figure shows that for $X_S/d = 0.75$ and $G_2/G_1 = 1$ the pressure drop coefficient is independent of staggering.

Correlation of the PIV data with the appropriate ΔP data suggests that there is a link between the variations in the upstream flow field and pressure drop. Examination of Figs. 12–15 shows that for $X_S/d \geqslant 0.75$ there was no change in pressure drop, regardless of the second row configuration. The corresponding PIV data show that the flow

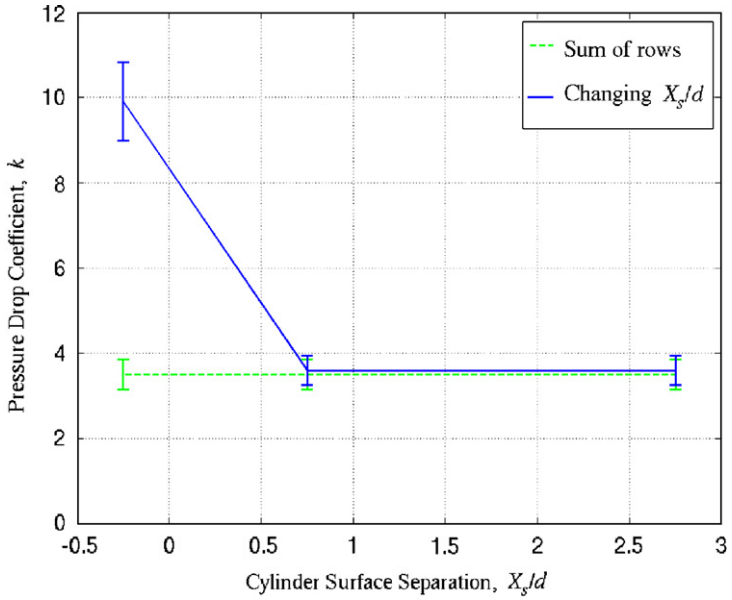

Fig. 15. Pressure drop coefficient as a function of X_S/d with $D/d = 1.5$, $G_2/G_1 = 2$, $Y/G_1 = 0.5$ at Re = 65.

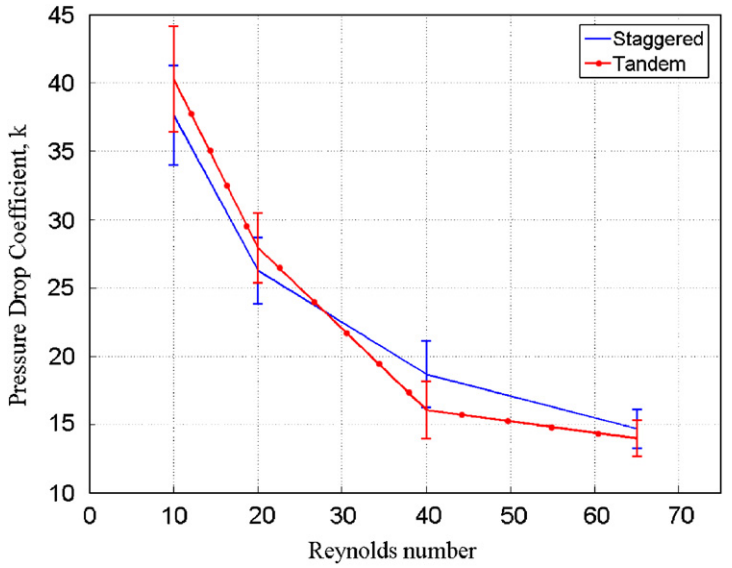

Fig. 16. Comparison of pressure drop coefficient as a function of Re through a bank of cylinders with $D/d = 1.5$, $G_2/G_1 = 1$, $X_S/d = 0.75$ and two staggerings.

field upstream of these configurations remained the same as that of one row of cylinders. This indicates that, when $\Delta P \rightarrow \sum \Delta P_{rows}$, the upstream flow field is likely to be the same as that through a single row of cylinders.

6. H_2 bubble visualization results

Hydrogen bubbles were used to visualize the upstream flow field that corresponds to the data in Fig. 15.

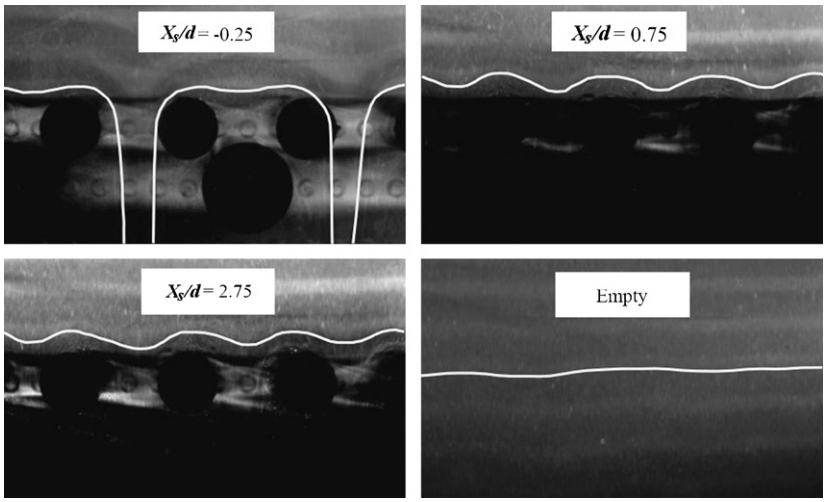

Fig. 17. The upstream flow field for various X_S/d and $D/d = 1.5$, $G_2/G_1 = 2$, $Y/G_1 = 0.5$ at $\mathrm{Re} = 65$.

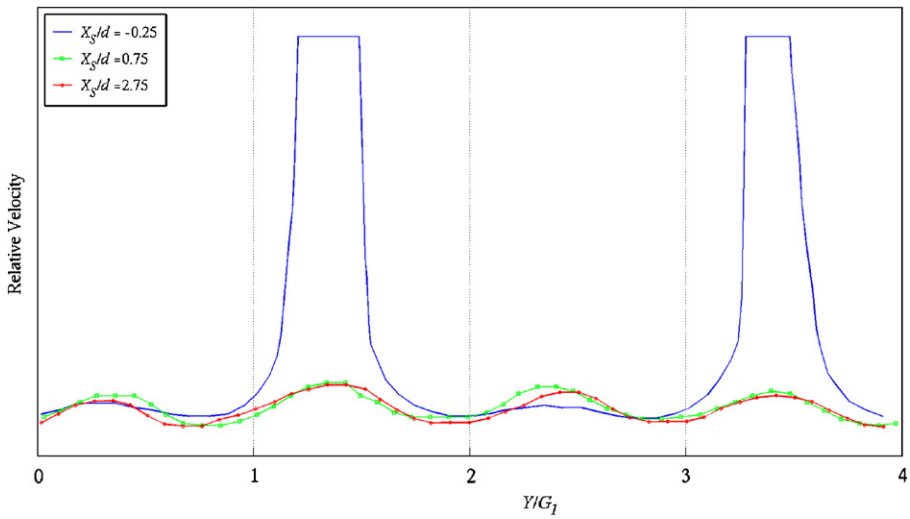

Fig. 18. The digitized data for the flow fields in Fig. 17.

Fig. 17 shows four images that display relative velocities for three different configurations of cylinders. The first three images correspond to the data points shown in Fig. 15. The fourth image is of the empty test-section. The leading edge of the bubble lines was highlighted, digitized and overlaid for comparison (Fig. 18). These hydrogen bubble visualizations are consistent with the PIV and pressure drop data measurements: for $X_S/d \geqslant 0.75$, all flow fields appear the same upstream of the bank of cylinders.

7. Conclusions

From the data it can be shown that for $X_S/d \geqslant 0.75$, the downstream row configuration had little or no effect on the upstream flow field or the overall pressure drop through the bank of cylinders. This indicates that the flow approaching the upstream row of cylinders is essentially independent of the downstream row.

In addition to the above, certain conclusions can be drawn in the context of the work of Sumner and Alam discussed in the literature review. These references addressed flow fields at Reynolds numbers where Kármán vortices were being

shed. They showed that when the wake of the upstream cylinder formed independently from the presence of the downstream cylinder, a step change in drag coefficient occurred. Further, following the step change, the drag coefficient plateaued with no significant change as cylinder separation increased. In the current study, Reynolds numbers are below what is expected to produce Kármán vortices and as a result the cylinder separation after which the upstream cylinder wake will form independently of the presence of the downstream cylinder is expected to reduce. The distance at which this occurs will be accompanied by a change in cylinder drag and consequently in flow field pressure drop. The pressure drop measurements show that it plateaus once a cylinder surface separation of $0.75d$ is reached. This levelling of the pressure drop is accompanied by a change in the upstream flow field wherein the inflow pattern becomes identical to that of a single row of cylinders. From these results, it is concluded that at both high and low Reynolds number levelling of the pressure drop indicates that the flow around the upstream cylinders becomes independent of the downstream cylinders and the inflow will be the same as for a single row of cylinders.

In the context of a multi-layer papermaking forming fabric these experimental results imply that the portion of the paper-side flow field attributable to the machine side, CD filaments will be negligible provided the machine-side filaments are at least $0.75d$ away from the paper-side filaments. Additionally, when the pressure drop of the multi-layered forming fabric is equal to the sum of its component layers' pressure drops the paper-side flow field will be the same as that of just the top fabric layer.

References

Adanur, S., 1994. Effects of forming fabric structural parameters on sheet properties. Tappi Journal 77, 187–195.

Alam, M., Moriya, M., Takai, K., Sakamoto, H., 2003. Fluctuating fluid forces acting on two circular cylinders in a tandem arrangement at a subcritical Reynolds number. Journal of Wind Engineering and Industrial Aerodynamics 91, 139–154.

Bearman, P., Wadcock, A., 1973. The interaction between a pair of circular cylinders normal to a stream. Journal of Fluid Mechanics 61, 499–511.

Beran, R., 1979. The evaluation and selection of forming fabrics. Tappi 62, 39–44.

Braun, M., 1995. Fluid flow structures in staggered banks of cylinders located in a channel. ASME Journal of Fluids Engineering 117, 36–44.

Dalpke, B., Kerekes, R., Green, S., 2004. Modelling jet impingement and the initial drainage zone in roll forming. Journal of Pulp and Paper Science 30, 65–70.

Gal, P.L., Chauvre, M.P., Takeda, Y., 1996. Collective behaviour of wakes downstream a row of cylinders. Physics of Fluids 8, 2097–2106.

Huang, Z., Olson, J., Kerekes, R., Green, S., 2006. Numerical simulation of the flow around rows of cylinders. Computers & Fluids 35, 485–491.

Huang, Z., 2003. Numerical simulations of flow through model paper machine forming fabrics. Master's Thesis, The University of British Columbia, Vancouver, British Columbia, Canada.

Iwaki, C., Cheong, K., Monji, H., Matsui, G., 2004. PIV measurement of the vertical cross-flow structure over tube bundles. Experiments in Fluids 37, 350–363.

Helle, T., 1978. How forming fabric design affects drainage and release. Pulp & Paper Canada 79, 91–98.

Johnson, D., 1986. Retention and drainage of multi-layer fabrics. Pulp & Paper Canada 87, 56–59.

Kim, H., Durbin, P., 1988. Investigation of the flow between a pair of circular cylinders in the flopping regime. Journal of Fluid Mechanics 196, 431–448.

Olson, J.A., 2002. Analytic estimate of the fibre orientation distribution in a headbox flow. Nordic Pulp and Paper Research Journal 17, 302–306.

Parker, J.D., 1972. The Sheet-Forming Process. Tappi Press, Atlanta, GA.

Polak, D., Weaver, D., 1995. Vortex shedding in normal triangular tube arrays. Journal of Fluids and Structures 9, 1–17.

Roychowdhury, D.G., Das, S.K., Sundararajan, T., 2002. Numerical simulation of laminar flow and heat transfer over banks of staggered cylinders. International Journal for Numerical Methods in Fluids 39, 23–40.

Sumner, D., Wong, S., Price, S., Païdoussis, M., 1999. Fluid behaviour of side-by-side circular cylinders in steady cross-flow. Journal of Fluids and Structures 13, 309–338.

Sumner, D., Price, S., Païdoussis, M., 2000. Flow-pattern identification for two staggered circular cylinders in cross-flow. Journal of Fluid Mechanics 411, 263–303.

Williamson, C., 1985. Evolution of a single wake behind a pair of bluff bodies. Journal of Fluid Mechanics 159, 1–18.

Ziada, S., 2000. Flow periodicity and acoustic resonance in parallel triangle tube bundles. Journal of Fluids and Structures 14, 197–219.